Civil Engineering Dimension
https://ced.petra.ac.id

Experimental Study on the Hysteretic Behavior of Tempered Steel Helical Dampers

Hakristuti, M.A.[1], Priyosulistyo, H.[1], Setiawan, A.F.[1]*, and Emilidardi, A.M.[1]
[1] Department of Civil and Environmental Engineering, Universitas Gadjah Mada, Yogyakarta
Jalan Grafika No. 2 Yogyakarta, INDONESIA

DOI: https://doi.org/10.9744/ced.28.2.264-275

Article Info:
Submitted: Oct 27, 2025
Reviewed: Dec 04, 2025
Accepted: Aug 12, 2026

Keywords:
steel helical spring,
damper,
heat treatment,
cyclic loading,
damping.

Corresponding Author:
Setiawan, A.F.
Department of Civil and Environmental Engineering, Universitas Gadjah Mada, Yogyakarta, Jalan Grafika No. 2 Yogyakarta, INDONESIA
Email: angga.fajar.s@ugm.ac.id

Abstract

Structural mitigation is a key strategy for reducing earthquake-induced property damage and casualties. Among various mitigation measures, dampers are widely used to enhance structural energy dissipation. This study proposes a heat-treated steel helical spring damper to improve damping performance. The dampers were fabricated from mild reinforcing steel bars with diameters of 6, 10, and 12 mm and different numbers of coils. An annealing process was applied to reduce the steel yield strength. The specimens were subjected to displacement-controlled sinusoidal cyclic loading to evaluate stiffness, strength, energy dissipation, and equivalent viscous damping ratio (EVDR). The results showed that reducing yield strength through annealing increased the EVDR by approximately 2.6%. Furthermore, larger coil diameters provided higher load-carrying capacity and greater energy dissipation. Conversely, increasing the number of coils reduced energy dissipation because of lower stiffness and larger yielding displacements within the applied loading range.

INTRODUCTION

Medium- and severe-earthquakes can cause significant damage to buildings, ranging from architectural elements to structural components, resulting in casualties. Hence, it is necessary to develop methods to increase the resilience of buildings against earthquakes. Several methods have been developed to mitigate potential damage to buildings through structural mitigation measures, repairs, and strengthening. One method is retrofitting, which involves adding steel bracing and a damper to damp earthquake vibrations. Along with technological developments, various types of dampers have been developed, significantly impacting the resilience of building structures against earthquakes. An example of a damper is a metallic damper, which dissipates energy through inelastic deformation and benefits from a stable hysteresis loop and resistance to changes in ambient temperature [1,2]. A shear panel damper is one type of metallic yield damper that utilises high-ductility, low-yield-strength steel material [3-5]. Further development of the shear panel damper type is designed to accommodate multidirectional loads in its application to bridge structures [6-10]. Another example of a damper is a friction damper, which provide energy dissipation from the friction between two solid bodies [11]. The current application of friction dampers in building structures is because they can serve as energy-dissipation devices, providing insulation [12,13]. Another example of a damper that employs a mechanism highly unaffected by stiffness is the viscoelastic damper. This damper is capable of dissipating earthquake energy across a range of vibrations, where the damper system is susceptible to variations in temperature and loading frequency [14,15].

Note : Discussion is expected before November, 1st 2026, and will be published in the "Civil Engineering Dimension", volume 29, number 1, March 2027.
ISSN : 1410-9530 print / 1979-570X online
Published by : **Petra Christian University**

A helical spring is a type of vibration-isolation device commonly used in vehicles to reduce shock and vibration. Although many helical springs are used as elastic springs in vehicles, they are also employed as isolation systems, energy-dissipation devices, or shock absorbers. In the vehicle's suspension system, a helical spring can temporarily store strain energy when a load is applied within its elastic range. Its purpose is to isolate the vehicle from vibration by shifting the natural period. In the implementation of a helical spring as a damper in the piping system of a nuclear power plant by Cho et al. [16], the steel coil damper (SCD) enables the piping system to remain in an elastic state under earthquake excitation due to hysteretic energy dissipation [16]. The research by Chang et al. [14] and Cho et al. [16] demonstrated that the yield strength, first stiffness, and second stiffness of SCD, as determined by both experimental and numerical results, show good agreement [17]. Conceptually, the nonlinear behavior of a steel coil or helical spring damper is affected by the steel material's yield strength and ductility. The helical spring damper is composed of a ductile material, enabling early energy dissipation and allowing for a large ultimate displacement. One method of obtaining steel with low yield strength and high ductility is tempering ordinary steel [18].

The mechanical properties of steel are related to its microstructure, which is obtained through various heat treatments. A slow cooling rate after the tempering process affects mechanical properties by influencing the microstructure [18,19]. Steel undergoing slow cooling treatment has lower yield strength but higher percentage elongation [20,21]. This happens because, at a fast cooling rate, martensite in carbon steel is in a hard, brittle phase, resulting in increased hardness and strength while reducing the specimen's ductility. The decrease in yield strength is also due to the coarser ferrite and pearlite dominating the microstructure, which allows them to move easier and consequently reduces hardness. The deformation temperature also affects the mechanical properties of steel. The yield strength and tensile strength of steel decreased as the tempering temperature increased [22-24]. Increasing the tempering temperature coarsens the steel's microstructure and carbides, while reducing stress on the martensite lowers the steel's hardness and strength. Based on these findings, the tempering method with a slow cooling rate has the potential to transform mild reinforcing steel bars into high-ductility, low-yield steel, thereby enabling their use as earthquake-damper devices. One possible utilization of reinforcing steel as an earthquake damper is the helical spring damper. There has been no study that discusses the hysteretic performance of tempered mild steel helical rebar spring dampers, which could potentially lead to further utilisation of mild reinforcing steel bars as a damper device. Therefore, an experimental study on the hysteretic behavior of steel helical spring dampers (SHSD) that considers tempering treatment is needed.

This paper investigates the effect of various spring coil parameters on the hysteretic behavior of helical rebar spring dampers under cyclic loading. Additionally, the effects of tempering treatment and different loading frequencies were investigated to examine their impact on hysteretic behaviour. In this experimental study, the optimal performance parameters of the helical rebar spring damper, specifically yield strength, yield displacement, and EVDR, are expected to be determined.

THEORETICAL BACKGROUND

In the design of a helical rebar spring damper, the spring's stiffness and force depend on the dimension parameters of the steel spring. They include the diameter of the rebar spring (d), the number of turns/coils (n), and the helical diameter (D) [25,26]. In the spring damper subjected to a force (F), as shown in Figure 1, the force (F) and torque (T) are directly related. The magnitude of the maximum shear stress of the spring damper is obtained from the combination of direct shear stress and torsional shear stress, as shown in Equation 1 [27] by substituting $\tau_{max} = \tau$, $T = FD/2$, $r = d/2$, $\tau_{max} = \pi d^4/32$, and $A = \pi d^2/4$, the following Equation 2 is obtained. In these formulations, the parameter Ks is introduced as the shear stress correction factor. This factor accounts for the additional shear stresses induced by the curvature of the spring wire and the direct shear force, which are not captured in the basic torsion formula. Using Castigliano's theorem, axial yield strength (F) can be determined by means of Equation (3).

$$\tau_{max} = \frac{Tr}{J} + \frac{F}{A} \tag{1}$$

$$\tau_{max} = \frac{8FD}{\pi d^3} + \frac{4F}{\pi d^2} \tag{2}$$

$$F = \frac{\tau \pi d^3}{8K_s D^3} \tag{3}$$

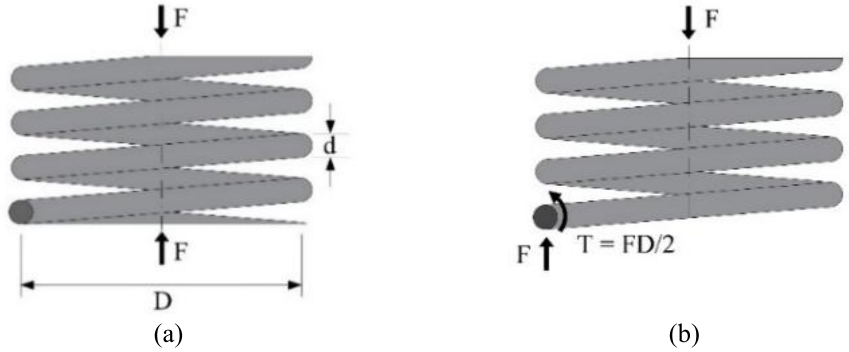

Figure 1. (a) Helical Spring with Axial Loading, and (b) Free Body Diagram of Direct Shear Stress and Torsional Shear Stress

MATERIALS PROPERTIES AND SPECIMEN PREPARATION

Materials

The Steel Helical Spring Damper (SHSD) specimens were fabricated from mild reinforcing steel bars, formed into coils with variations in bar diameter, number of coils, and heat treatment conditions, as illustrated in Figure 2(a). The bar diameters of the spring dampers were 6, 10, and 12 mm, with 1 to 3 active coils. The specimens were produced by winding the steel bars around a cylindrical mandrel with a diameter of 24.5 mm to achieve the helical configuration. Consequently, a total of 18 specimens (3 × 3 × 2) were used in this experiment, as summarized in Table 1. Furthermore, the specimen designation is based on the material model (NT for non-heat-treated or WT for heat-treated), followed by the bar diameter and the number of coils.

Heat Treatment

The heat treatment of the SHSD specimens was conducted in a furnace constructed from refractory bricks with a chamber measuring 10 cm x 20 cm, as shown in Figure 2(b). The specimens were heated to a soaking temperature of approximately 800°C and held for 25 minutes, as illustrated in Figure 2(c). Following the heating phase, the furnace was sealed using a layer of aluminum foil and refractory bricks to facilitate slow cooling within the chamber. This heat treatment sequence is detailed in Figure 2 and the resulting temperature decay was recorded. The specimens were designated as WT (With Treatment) and NT (Non-Treatment) to distinguish between the heat-treated and non-heat-treated helical springs, respectively.

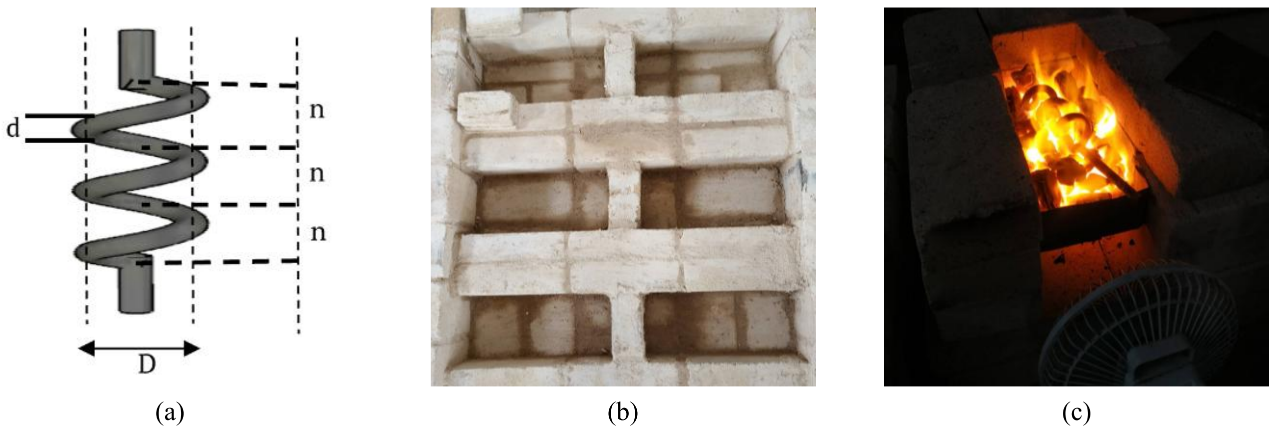

Figure 2. Information about SHSD; (a) Dimension Parameters, (b) Heating Furnace, and (c) Heating Process

Table 1. Design Parameters of the Steel Helical Spring Damper

Parameters	Analytical case	Number of cases
Material model	Non-heat treatment (NT) and with heat treatment (WT)	2
Bar diameter	6, 10, 12 mm	3
Number of coils	1, 2, 3	3
Total cases		18

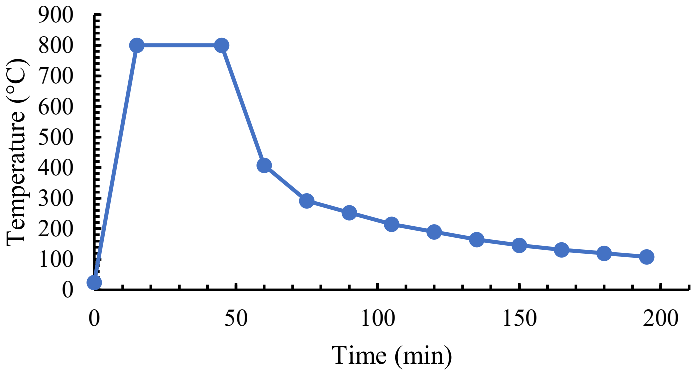

Figure 3. Heat Treatment Sequence

EXPERIMENTAL PROCEDURE

The mechanical properties of the steel bar, specifically its yield stress and maximum elongation, were evaluated through uniaxial tension tests before the assembly of the helical spring dampers. Cyclic loading of helical rebar spring damper specimens was conducted under displacement control. The cyclic displacement load is applied using a dynamic sinusoidal procedure on a shaking table at 0.5 Hz and 1.0 Hz. To achieve lateral restraint, the specimen was placed on a 24.5mm cylindrical pipe and connected by welding. The movable drive shaft and sleeve are welded connected to the coil spring specimen and have relative displacement to the fixed sleeve. Therefore, the axial force resist and deformation only occurred on the coil spring specimens. The specimen was then secured on one side using nuts and bolts to prevent movement when loaded. The loading setup configuration of the specimens is shown in Figure 4.

The cyclic loading test was conducted to obtain the stiffness, yield strength, yield displacement, and equivalent viscous damping ratio (EVDR). The equipment used includes a load cell to measure load and an LVDT to measure displacement. All recording devices are connected to DEWE-43 and Dewesoft software version 3.12. The dynamic load excitation was generated by the shaking table that was connected to the right end of the specimen. A load cell was installed between the shaking table and the specimen, connected via a cylindrical steel pin to prevent moment transfer during loading. The LVDT with a fixed support was placed toward the shaking table to measure the displacement of the spring damper.

During specimen loading, a sinusoidal signal at 0.5 Hz and 1 Hz was applied as the cyclic load. The loading consists of several cycles grouped into displacement control blocks. Each block has a specific displacement target, i.e., 2, 4, 6, 8, 10, 15, 20, and 25 mm, named as DT2, DT4, DT6, DT8, DT10, DT15, DT20, and DT25, respectively. The cyclic loading protocol for the different numbers of specimen coils is shown in Table 2. The maximum displacement targets for one, two, and three coils are 15 mm, 20 mm, and 25 mm, respectively. The reason is that helical rebar spring dampers with higher coil numbers generate larger elongation capacity. At the loading stage, with a frequency of 0.5 Hz, ten cycles were performed using four precursors and five signals, as directed by the displacement target, as shown in Figure 5. The precursor signal is needed to stabilize the movement on the shaking table.

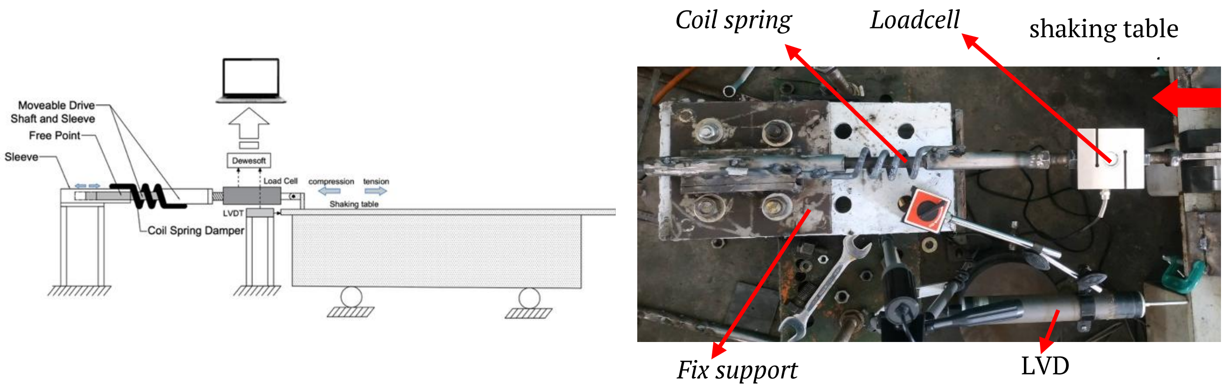

(a) (b)

Figure 4. Loading Set Up the Configuration of the Specimens: (a) Schematic, and (b) Implementation

Table 2. Cyclic Loading Protocol and Displacement Targets for Varying Coil Numbers

Number of coils	Displacement target							
	DT2	DT4	DT6	DT8	DT10	DT15	DT20	DT25
1	√	√	√	√	√	√		
2	√	√	√	√	√	√	√	
3	√	√	√	√	√	√	√	√

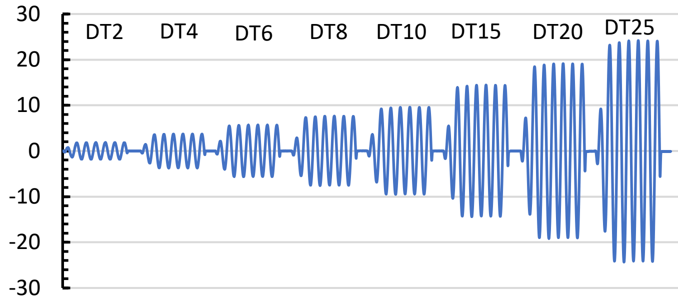

Figure 5. Cyclic Loading Protocol Blocks

RESULTS AND DISCUSSION

Tensile Test Result

The tensile test results indicated that the tempering treatment may have reduced the steel bar's yield strength, as illustrated in Figure 6. The yield strength and total elongation results for each bar of specimens were presented in Table 3. It should be noted that the results for the 6 mm, 10 mm, 12 mm bars were derived from single data points. Following the heat treatment, a decrease in yield strength was observed across all specimens. Specifically, the yield strength of the 6 mm specimens decreased from 335.41 MPa to 256.85 MPa, representing a 23.42% reduction. In the 10 mm specimens, a 1.87% decrease (from 402.16 MPa to 394.64 MPa) was recorded, while the 12 mm specimens exhibited a 6.02% reduction.

The reduction in the yield strength was attributed to heat treatment with a slow cooling rate. During tempering, a diffusion process occurred in which carbon could escape from the martensite, as evidenced by the study of Hansu and Güneyisi [15]. Increasing the tempering temperature accelerated the diffusion rate and the enlargement rate of cementite particles. The enlargement of the cementite particles decreased the steel's yield strength. This was consistent with the test results for specimens WT6, WT10, and WT12, in which the steel bar exhibited a reduction in yield strength, as shown in Figure 6(b). The smallest percentage decrease occurred in the DP12 specimen. The reason for this discrepancy was the difference in the volume of reinforcing steel specimens. Specimens with a larger diameter or volume per unit length required slower heat treatment. Consequently, the rate of diffusion that occurred was also slower. The reduction in yield strength is a critical factor in the performance of the spring helical damper, by enabling earlier plastic deformation, the damper achieves plumper hysteretic loops relative to its elastic capacity. Although the absolute force capacity is lower, this behavior directly enhances the damping efficiency, resulting in a higher Equivalent Viscous Damping Ratio (EVDR) for the heat-treated specimens.

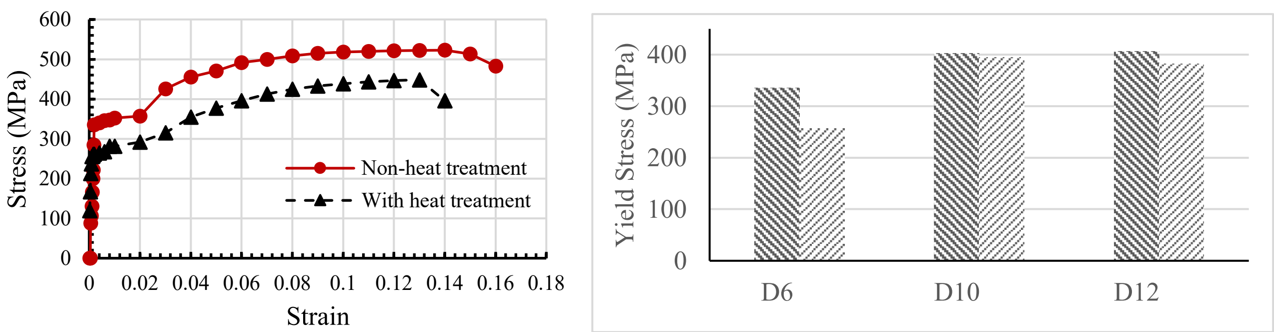

(a) (b)

Figure 6. Uniaxial Test Results of Rebar Material: (a) Stress-Strain Curve of Rebar with a 6 mm Diameter, and (b) Comparison of Yield Strength between Before and After Heat Treatment

Table 3. Yield Strength and Elongation

Rebar diameter (mm)	Case	Yield strength, f_y (MPa)	Total elongation (%)
6	Non-heat treatment (NT)	335.41	16
	With heat treatment (WT)	256.85	15
10	Non-heat treatment (NT)	402.16	16
	With heat treatment (WT)	394.64	18
12	Non-heat treatment (NT)	406.66	10
	With heat treatment (WT)	382.17	21

Cyclic Test Result

Table 4. Equivalent Viscous Damping Ratio (EVDR, %)

Specimen	Displacement control (mm)															
	Loading frequency 0.5 Hz								Loading frequency 1.0 Hz							
	2	4	6	8	10	15	20	25	2	4	6	8	10	15	20	25
NT6-1coil	2.0	3.7	10.8	17.5	22.7	31.6	-	-	1.6	5.8	18.7	18.7	22.5	28.1	-	-
WT6-1coilPen	7.3	8.5	17.3	23.7	28.5	35.9	-	-	7.4	9.3	18.0	25.6	31.4	38.8	-	-
NT6-2coil	3.8	2.4	2.7	5.6	9.3	18.7	24.4	-	4.0	2.4	2.9	6.3	10.4	19.8	26.3	-
WT6-2coil	3.6	6.6	14.6	21.5	26.5	34.0	37.4	-	3.6	6.8	15.8	22.5	27.9	36.2	40.7	-
NT6-3coil	2.3	1.1	1.2	2.6	5.1	13.2	20.1	20.3	1.3	1.0	1.5	3.5	6.7	14.1	20.6	26.3
WT6-3coil	2.2	2.2	5.9	11.4	16.9	27.4	31.7	34.9	2.2	2.1	6.3	12.6	18.4	30.6	38.0	41.2
NT10-1coil	1.8	8.9	17.6	25.4	28.8	35.2	-	-	1.7	10.3	19.2	25.7	30.2	37.4	-	-
WT10-1coil	2.6	1.3	25.9	31.5	35.3	41.0	-	-	2.8	16.7	26.6	32.3	35.8	40.7	-	-
NT10-2coil	1.3	2.1	8.0	15.1	20.9	29.3	33.8	-	1.4	2.3	8.9	16.5	22.5	30.5	35.6	-
WT10-2coil	1.2	2.7	10.2	18.0	23.1	31.9	35.9	-	1.2	3.2	11.1	19.1	24.3	32.2	36.7	-
NT10-3coil	1.3	1.2	3.5	8.2	13.5	24.3	29.9	33.2	1.2	1.2	3.9	9.6	14.9	24.8	31.4	34.1
WT10-3coil	0.9	1.7	7.3	14.2	19.3	28.4	32.9	37.0	1.0	1.9	7.9	15.3	20.6	29.6	34.4	36.7
NT12-1coil	1.9	10.7	21.5	28.1	32.0	39.5	-	-	1.8	10.9	22.1	28.8	33.3	39.5	-	-
WT12-1coil	2.1	15.2	25.6	31.3	35.4	41.4	-	-	2.3	15.7	26.0	31.6	35.4	41.2	-	-
NT12-2coil	1.2	2.4	9.0	17.1	22.6	31.8	36.5	-	1.2	2.7	9.9	18.0	19.4	32.5	39.7	-
WT12-2coil	1.4	5.4	13.8	21.4	26.5	35.1	39.8	-	1.4	5.5	14.4	22.1	27.6	35.5	39.5	-
NT12-3coil	1.1	1.2	4.6	10.7	16.8	28.0	34.0	37.4	1.2	1.1	5.1	11.9	18.3	28.5	34.1	37.5
WT12-3coil	1.5	3.8	9.2	16.0	21.7	30.3	35.4	38.3	1.4	4.0	10.0	17.1	24.1	31.2	36.3	39.3

Table 5. Axial Yield Strength

	Yield strength at 0.5 hz loading frequency (kN)		Difference (%)	Yield strength at 1.0 hz loading frequency (kN)		Difference (%)
	Experimental	Analytical		Experimental	Analytical	
NT6-1coil	0.59	0.58	-1.51	0.46	0.58	-26.81
WT6-1coilPen	0.34	0.37	8.77	0.36	0.37	-3.87
NT6-2coil	0.52	0.58	10.31	0.54	0.58	-8.62
WT6-2coil	0.36	0.37	4.00	0.38	0.37	-0.97
NT6-3coil	0.62	0.58	-6.42	0.60	0.58	-3.38
WT6-3coil	0.40	0.37	-6.69	0.42	0.37	-10.86
NT10-1coil	2.09	2.31	9.46	2.30	2.31	0.36
WT10-1coil	1.75	1.85	5.59	1.76	1.85	5.19
NT10-2coil	2.26	2.31	2.20	2.26	2.31	2.27
WT10-2coil	1.77	1.85	4.43	1.78	1.85	-3.89
NT10-3coil	2.24	2.31	2.86	2.25	2.31	2.57
WT10-3coil	1.70	1.85	8.21	1.71	1.85	7.67
NT12-1coil	3.78	3.77	-0.35	3.94	3.77	-4.46
WT12-1coil	3.23	3.52	8.37	3.24	3.52	8.13
NT12-2coil	3.83	3.77	-1.52	3.83	3.77	-1.49
WT12-2coil	3.49	3.52	1.02	3.47	3.52	1.48
NT12-3coil	3.85	3.77	-2.02	3.44	3.77	8.77
WT12-3coil	3.01	3.52	14.58	3.02	3.52	14.28

The experimental test revealed that the EVDR of each specimen varied with the determined variables, as illustrated in Table 4. These EVDR values were derived by averaging the EVDR for each cycle within each block. Generally, the distinct loading frequencies led to marginal differences in EVDR outcomes. Heat treatment improved EVDR performance compared to the untreated condition. An increase in the number of coils reduced energy dissipation by enhancing flexibility and increasing the yielding displacement. Furthermore, a larger bar diameter was associated with a higher EVDR attainment. Additionally, a larger displacement resulted in a higher EVDR, suggesting that the displacement load control remained below the strength degradation state.

Table 5 indicates that the yield strength of the spring damper was affected by the material of the specimen, the diameter of the coil, and the diameter of the spring bar. The axial yield strength state is determined based on the first significant slope change of the backbone curve, as referred to by Shen et al. [28]. Nevertheless, the discrepancy in loading frequency at 0.5 Hz and 1.0 Hz resulted in a marginal discrepancy in axial yield strength. The coil material exerted a significant influence on the axial yield strength value. The increase in the material's yield stress resulted in a corresponding increase in the axial yield strength of the spring damper. As illustrated in Table 5, the tested specimens showed variations in yield strength, indicating that those with identical coil and helical diameters differed in axial yield strength. The coil diameter affected axial yield strength, with specimens exhibiting higher axial yield strength at larger coil diameters. These results were compared with the calculation of axial yield strength using Equation (3), which yields a value close to the experimental result, demonstrating a comparable pattern as shown in the percentage difference figures in Table 5. Furthermore, the specimen employed the same cylinder diameter, thereby establishing a proportional increase in helical diameter as the spring bar diameter increased.

The Effect of Heat Treatment

According to Figure 7, the tempering treatment resulted in a lower yield strength. When displacement control was applied at 2, 4, 6, 8, 10, and 15 mm, the hysteresis loop of the heat-treated specimen was smaller than that of the non-heat-treated specimen. In the inelastic state, as shown in Figure 8(a) and (b), the force at the same displacement control was higher for the non-heat-treated specimen. Conversely, the elastic stiffness of each specimen was almost equal. The 12 mm diameter specimen with a single active coil served as a representative case for the various diameters and coil configurations, as other specimens exhibited similar behavioral patterns. Consequently, the specimens with tempering treatment exhibited a larger equal viscous damping ratio. This was because the heat-treated specimen reduced the steel's yield strength.

This phenomenon occurred because the reduced yield strength in the heat-treated specimens facilitated an earlier transition from the elastic to the plastic state during the loading cycles. As the yielding occurred at a lower load level, the heat-treated specimens spent a greater proportion of the displacement cycle dissipating energy through metallic yielding. This resulted in a 'plumper' hysteretic loop relative to the specimen's maximum force capacity, which significantly reduced the elastic strain energy (E_{el}) relative to the dissipated energy (E_d).

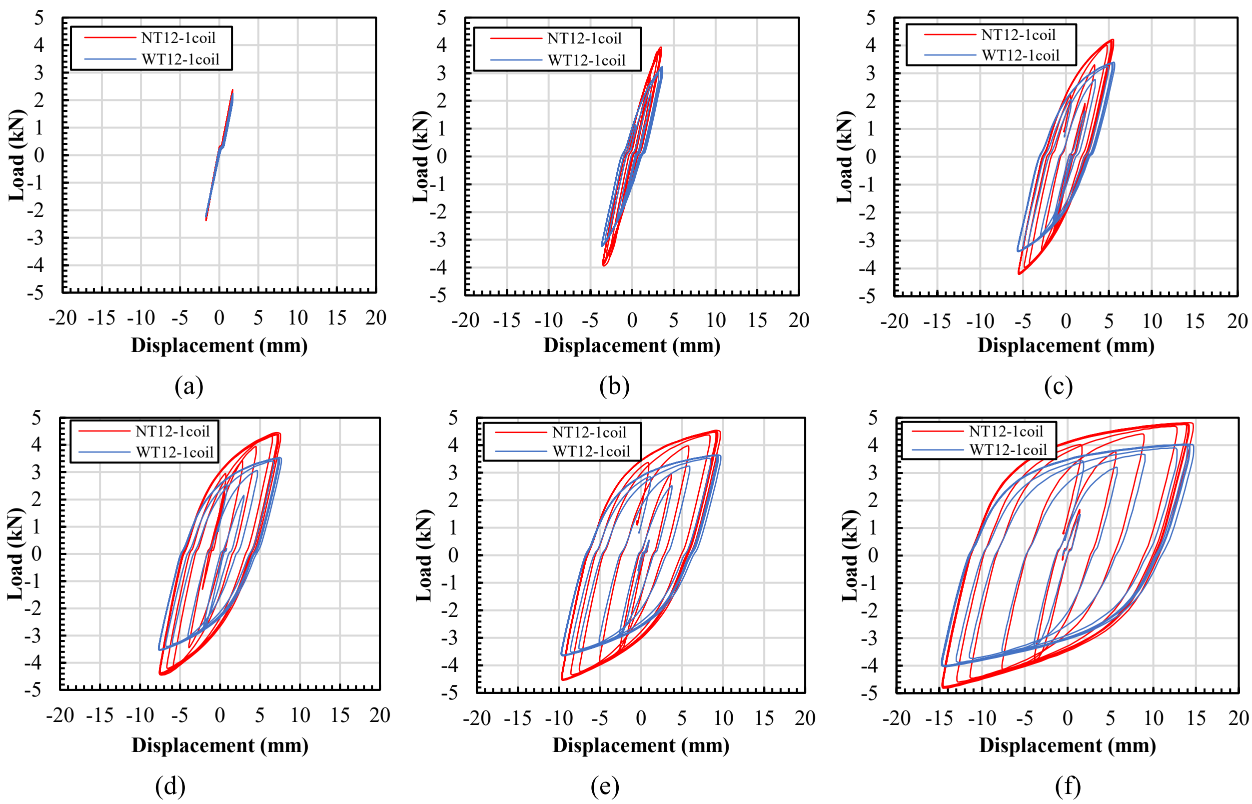

Figure 7. Hysteretic Loop of the NT12-1coil and WT12-1coil Specimen under Displacement Control; (a) 2 mm, (b) 4 mm, (c) 6 mm, (d) 8 mm, (e) 10 mm, and (f) 15 mm

The general trend observed was that the equivalent viscous damping ratio increased with displacement. The specimen with a diameter of 12 mm and one coil, as shown in Figure 8, could be considered to represent the difference in the EVDR value for each displacement. The heat-treated spring damper exhibited a higher damping ratio than the non-heat-treated spring damper. The increase in the equivalent viscous damping ratio of the heat-treated specimen was concurrent with that observed by He at al. [8], wherein specimens with lower yield strength exhibited plastic deformation in smaller deformation.

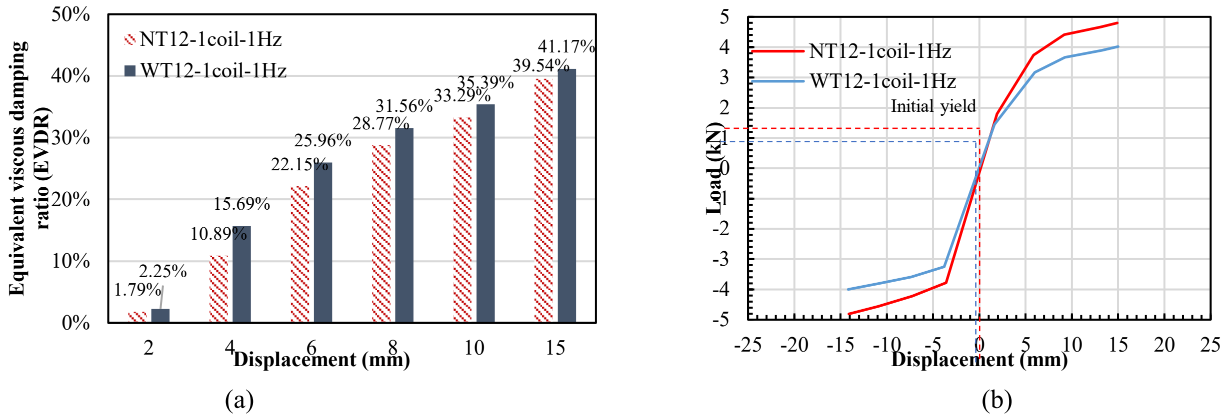

Figure 8. Comparison of (a) Equivalent Viscous Damping Ratio, and (b) Envelope Curve of the Specimen NT12-1coil and WT12-1coil

The Effect of Coil Numbers

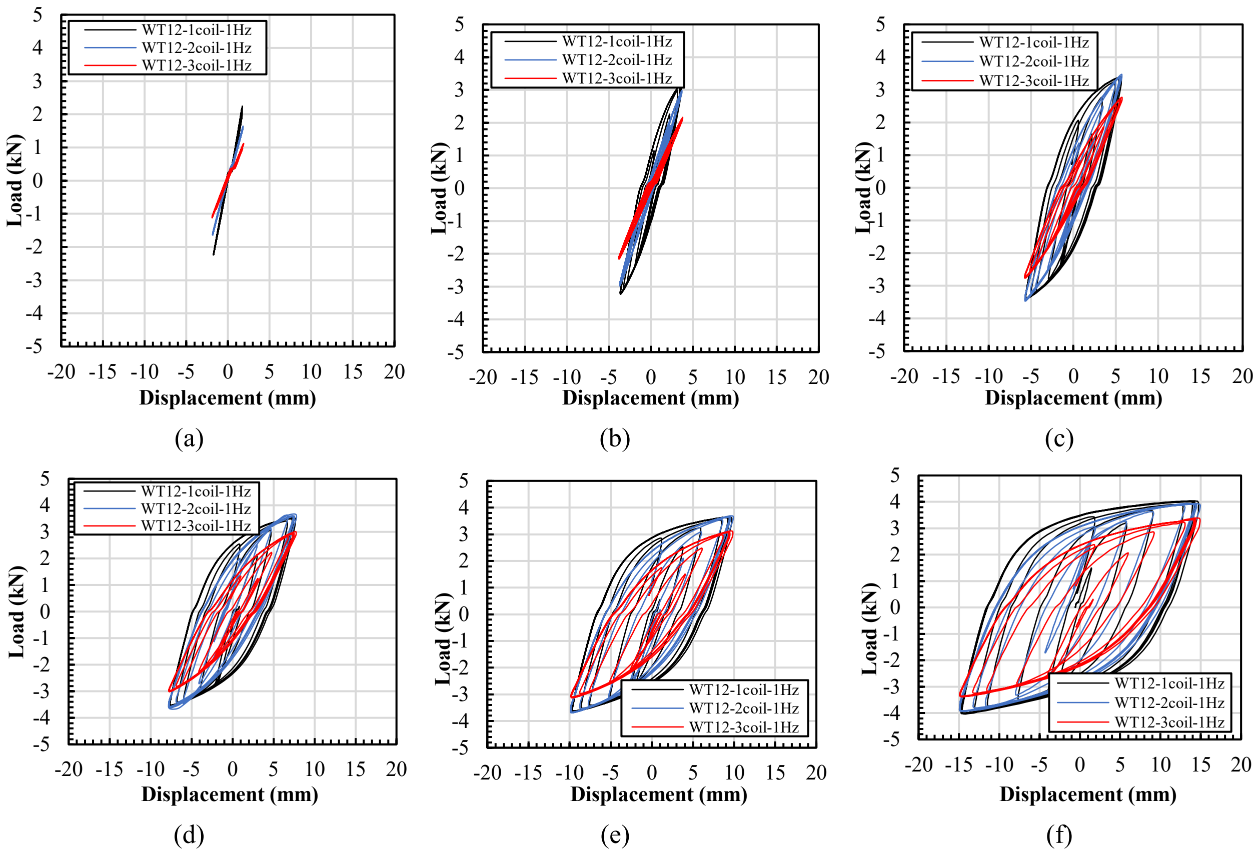

Figure 9. Hysteresis Loop for Specimen WT12-1coil, WT12-2coil, and WT12-3coil for Specimen under Displacement Control; (a) 2 mm, (b) 4 mm, (c) 6 mm, (d) 8 mm, (e) 10 mm, and (f) 15 mm

The hysteretic loop area decreased with increasing coil number, as shown in Figure 9 for specimens WT12-1coil, WT12-2coil, and WT12-3coil. The 12 mm diameter specimens served as a representative case for the other diameter variations, as the 6 mm and 10 mm specimens exhibited similar behavioral characteristics. Under the same deflection-controlled loading, all specimens exhibited comparable force levels. The backbone curves in Figure 10(a) indicate that the yield strength was nearly independent of the number of coils, whereas the yield deformation increased with increasing coil number. This behavior is consistent with the theoretical relationship given in Equation (1), which indicates that, for identical spring geometry, the strength is not governed by the number of coils; rather, the stiffness decreases with increasing number of coils due to greater elastic deformation.

Accordingly, the hysteretic loop area directly affected the equivalent viscous damping ratio (EVDR), which increased as the number of coils decreased, as shown in Figure 10(b). The single-coil specimen exhibited the highest EVDR, followed by two-coil and three-coil specimens. In general, higher stiffness and shorter yield displacement were the dominant factors contributing to a larger EVDR. However, the response at larger deformation levels could not be evaluated because the ultimate deformation capacity was not reached in the present tests. Further studies are therefore required to clarify whether increasing the number of coils improves hysteretic energy dissipation at large deformations or instead promotes instability, such as buckling.

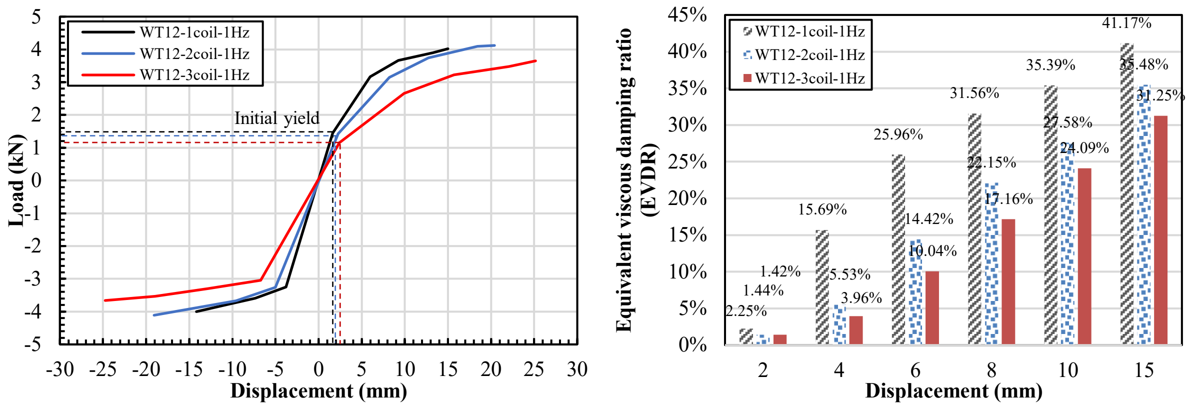

(a) (b)

Figure 10. Comparison of (a) Equivalent Viscous Damping Ratio, and (b) Envelope Curve of the Specimens WT12-1coil, WT12-2coil, and WT12-3coil

Correlation between Bar Diameter and Hysteretic Behavior

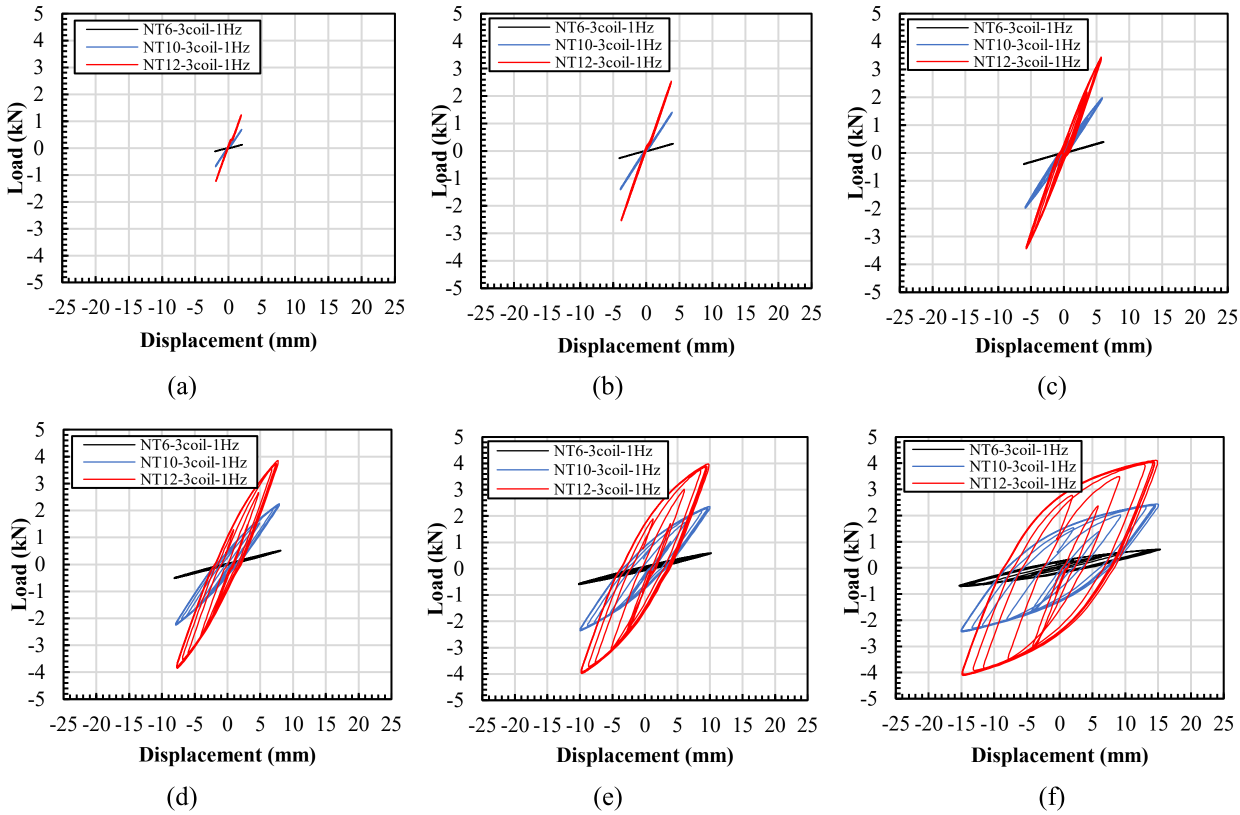

Figure 11. Hysteresis Loop for Specimen NT6-3coil, NT10-3coil, and NT12-3coil for Specimen under Displacement Control: a) 2 mm, b) 4 mm, c) 6 mm, d) 8 mm, e) 10 mm, and f) 15 mm

The general trend of the hysteretic loop area increased as the bar diameter of the specimen increased, as shown in Figure 11, which consisted of specimens NT6-3coil, NT10-3coil, and NT12-3coil. To isolate and compare the influence of bar diameter, the specimens with three active coils were selected as a representative configuration, with the 12 mm diameter specimen serving as the primary reference for the observed trends. At the same deflection control, the greatest force occurred on the specimen with a bar diameter of 12 mm, followed by 10 mm, and finally 6 mm. The axial yield strength, illustrated in Figure 12, was consistent with Eq. 5; it showed a positive correlation with increasing bar diameter. The increase in bar diameter also increased the stiffness rate of the spring under the same deflection. The greatest strength was observed in the specimen with a bar diameter of 12 mm, followed by 10 mm, and finally 6 mm. These observations confirmed fundamental mechanical principles, as the torsional resistance and load-carrying capacity of a helical spring are inherently governed by its wire diameter. It should be noted that while these results validated the experimental setup, the correlation between bar diameter and structural capacity is a well-established mechanical behavior.

In general, the equivalent viscous damping ratio increased in proportion to the bar diameter. Figure 12 illustrates the equivalent viscous damping ratio of the non-heat-treated specimen with three coil numbers on different bar diameters. This phenomenon occurred because the hysteretic loop area was larger in a specimen with fewer coils, resulting in the largest equivalent viscous damping ratio in the specimen with one coil. When subjected to the same force, the elastic displacement of the spring damper with a higher diameter was lower, and its initial stiffness was significantly larger than that of the other two dampers. The equivalent viscous damping ratio of the specimen with a larger bar diameter decreased in the elastic region but increased in the plastic region.

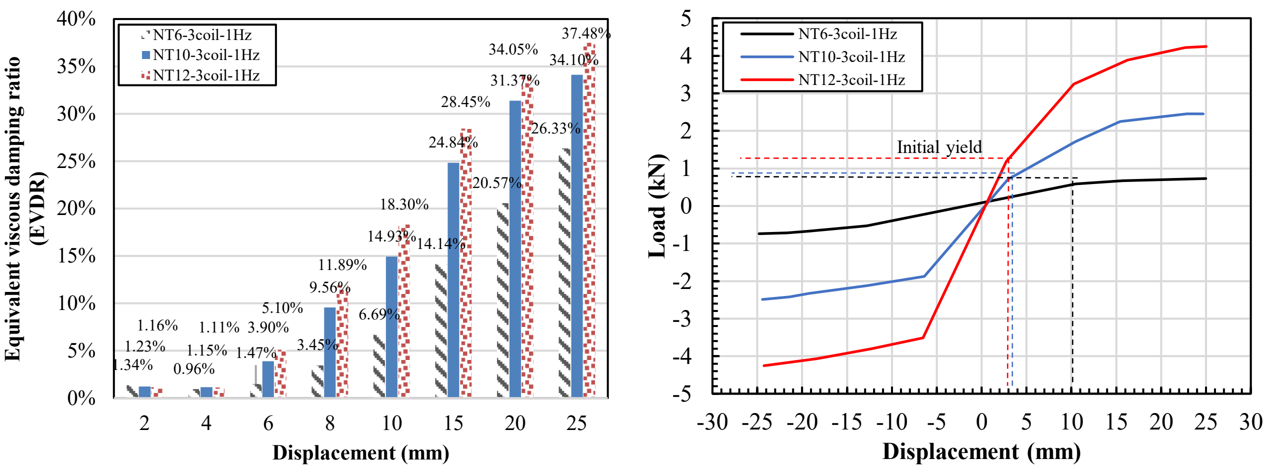

(a) (b)

Figure 12. (a) Equivalent Viscous Damping Ratio, and (b) Backbone Curve of the Specimen NT6-3coil, NT10-3coil, and NT12-3coil

CONCLUSIONS

This experimental study investigated the hysteretic behavior of helical spring dampers fabricated from reinforcing steel bars, focusing on the effects of material treatment and geometric parameters. The heat treatment, achieved through slow-cooling tempering, alters the material's mechanical properties to enhance its damping performance. The treatment was effective in reducing the axial yield strength of the steel bars, with a decrease of up to 35.74% observed in the 6 mm diameter specimens. This reduction in yield strength allows the damper to enter a plastic state at smaller deformations. Consequently, the heat-treated specimens consistently exhibited a higher EVDR than their untreated counterparts, indicating superior energy dissipation per unit displacement.

The damper's hysteretic behavior was also found to be highly dependent on its geometric parameters, specifically the number of coils and the bar diameter. The study revealed an inverse relationship between the number of coils and damping capacity: increasing the number of coils led to a lower EVDR. This occurs because additional coils increase the damper's flexibility and reduce its overall stiffness, resulting in a smaller hysteretic loop area and, consequently, less energy dissipation for the same displacement target. As the basic theorem, increasing the bar diameter improved mechanical performance. Larger-diameter bars provided greater yielding force resistance and stiffness, resulting in a larger hysteretic loop area and a significantly higher EVDR, demonstrating greater energy dissipation.

Furthermore, the study concluded that the performance of the helical spring damper is independent of the loading frequencies tested. The experimental results showed nearly identical EVDR values for tests conducted at 0.5 Hz and 1.0 Hz, suggesting the damper offers stable, predictable performance under low-frequency seismic vibrations. Considering all findings, the research proposes a practical application for this technology. While effective at dissipating energy, these helical spring dampers possess a relatively small force resistance capacity. This characteristic makes them particularly well-suited for use as energy dissipation devices in low- to medium-rise buildings, where high force resistance is less critical.

DISCLAIMER

The authors declare that they have no known competing financial interests or personal relationships that could have influenced the work in this article.

ACKNOWLEDGMENTS

Thanks are delivered to the Structural Laboratory of the Department of Civil and Environmental Engineering of the Engineering Faculty of Universitas Gadjah Mada for providing facilities, and great gratitude to the laboratory technicians who have supported this research come to fruition without any significant problems.

REFERENCES

1. Aghlara, R., Tahir, M.M., and Adnan, A., Comparative Study of Eight Metallic Yielding Dampers, *Jurnal Teknologi,* 77(16), 2015, pp. 119–125, doi: 10.11113/jt.v77.6408.
2. Suswanto, B., Ghifari, F., Triwulan, T., Sugihardjo, H., and Pangestuti, P.A., Performance Analysis of Eccentrically Braced Frames (EBF) using Metallic Yielding Damper (MYD) with Hysteretic Steel Damper (HSD) Type, *Civil Engineering Dimension*, 27(1), 2025, pp. 1–11, doi: 10.9744/ced.27.1.1-11.
3. Tanaka, K. and Sasaki, Y., Hysteretic Performance of Shear Panel Dampers of Ultra Low-Yield-Strength Steel for Seismic Response Control of Buildings, *Journal of Fujita Technical Research Institute*, 2000, pp. 1–8.
4. Xu, L.Y., Nie, X., and Fan, J.S., Cyclic Behaviour of Low-Yield-Point Steel Shear Panel Dampers, *Engineering Structures*, 126, 2016, pp. 391–404, doi: 10.1016/j.engstruct.2016.08.002.
5. Xu, L.Y., Tao, M.X., Nie, X., Fan, J.S., and Taciroglu, E., Modeling Techniques for Strain-Range-Dependent Hardening Behavior of Low-Yield-Point Steel Shear Panel Dampers, *Journal of Structural Engineering*, 143(12), 2017, p. 04017172, doi: 10.1061/(ASCE)ST.1943-541X.0001896.
6. Emilidardi, A.M., Fajar, A.S., Awaludin, A., Satyarno, I., and Sunarso, M., Numerical Model of Finned Tubular Shear Panel Damper for Multi-direction Seismic Excitation, *Proceedings of the 5th International Conference on Sustainable Civil Engineering Structures and Construction Materials*, Singapore, 2022, pp. 751–766, doi: 10.1007/978-981-16-7924-7_49.
7. Awaludin, A., Setiawan, A.F., Satyarno, I., Shuanglan, W., and Haroki, Y., Finite Element Analysis of Bi-directional Shear Panel Damper with Square Hollow Section under Monotonic Loading, *Journal of the Civil Engineering Forum,* 8, 2022, pp. 157–168, doi: 10.22146/jcef.3842.
8. Emilidardi, A.M., Awaludin, A., Triwoyono, A., Setiawan, A.F., Satyarno, I., and Santoso, A.K., Seismic Performance Enhancement of a PCI-Girder Bridge Pier with Shear Panel Damper Plus Gap Numerical Simulation, *Earthquakes and Structures*, 27(1), 2024, pp. 69–82, doi: 10.12989/eas.2024.27.1.069.
9. He, H., Wang, X., and Zhang, X., Energy-Dissipation Performance of Combined Low Yield Point Steel Plate Damper Based on Topology Optimization and Its Application in Structural Control, *Advances in Materials Science and Engineering*, 2016, 2016, doi: 10.1155/2016/5654619.
10. Haroki, Y., Awaludin, A., Priyosulistyo, H., Setiawan, A.F., and Satyarno, I., Seismic Performance Comparison of Simply Supported Hollow Slab on Pile Group Structure with Different Operational Category and Shear Panel Damper Application, *Civil Engineering Dimension*, 25(1), 2023, pp. 10–19, doi: 10.9744/ced.25.1.10-19.
11. Setiawan, A.F. and Takahashi, Y., A High Seismic Performance Concept of Integrated Bridge Pier With Triple RC Columns Accompanied by Friction Damper Plus Gap, *Journal of Japan Society of Civil Engineers, Series A1 (Structural Engineering and Earthquake Engineering),* 74(4), 2018, pp. I_131–I_147, doi: 10.2208/jscejseee.74.i_131.
12. Becker, T.C., *Advanced Modeling of the Performance of Structures Supported on Triple Friction Pendulum Bearings*, Ph.D. Dissertation, Department of Civil and Environmental Engineering, University of California, Berkeley, Berkeley, CA, USA, 2011.

13. Becker, T.C., Bao, Y., and Mahin, S.A., Extreme Behavior in a Triple Friction Pendulum Isolated Frame, *Earthquake Engineering and Structural Dynamics*, 46(15), 2017, pp. 2683–2698, doi: 10.1002/eqe.2924.
14. Chang, K.C., Soong, T.T., Lai, M.L., and Nielsen, E.J., Viscoelastic Dampers as Energy Dissipation Devices for Seismic Applications, *Earthquake Spectra*, 9(3), 1993, pp. 371–387, doi: 10.1193/1.1585721.
15. Hansu, O. and Güneyisi, E., Comparison of Novel Seismic Protection Devices to Attenuate the Earthquake Induced Energy, *Actuators,* 10, 2021.
16. Cho, S.G., Furuya, O., and Kurabayashi, H., Enhancement of Seismic Resilience of Piping Systems in Nuclear Power Plants Using Steel Coil Damper, *Nuclear Engineering and Design*, 350, 2019, pp. 147–157, doi: 10.1016/j.nucengdes.2019.05.006.
17. Chang, S. and Cho, S.G., An Intelligent Process to Estimate the Nonlinear Behaviors of an Elasto-Plastic Steel Coil Damper Using Artificial Neural Networks, *Actuators*, 11(1), 2022, doi: 10.3390/act11010009.
18. Thelning, K.E., *Steel and Its Heat Treatment*, Butterworth, 1966.
19. Dieter, G.E., *Mechanical Metallurgy*, Second Edition, McGraw-Hill, USA, 1976.
20. Rasouli, D., Khameneh Asl, S., Akbarzadeh, A., and Daneshi, G.H., Effect of Cooling Rate on the Microstructure and Mechanical Properties of Microalloyed Forging Steel, *Journal of Materials Processing Technology*, 206(1–3), 2008, pp. 92–98, doi: 10.1016/j.jmatprotec.2007.12.006.
21. Equbal, M.I., Alam, P., Ohdar, R., Anand, K.A., and Alam, M.S., Effect of Cooling Rate on the Microstructure and Mechanical Properties of Medium Carbon Steel, *International Journal of Metallurgical Engineering*, 5(2), 2016, pp. 21–24, doi: 10.5923/j.ijmee.20160502.01.
22. Tukur, S.A., Usman, M.M., Muhammad, I., and Sulaiman, N.A., Effect of Tempering Temperature on Mechanical Properties of Medium Carbon Steel, *International Journal of Engineering Trends and Technology*, 9(15), 2014, p. 15, doi: 10.14445/22315381/IJETT-V9P350.
23. Zhu, Y., Li, Y., Fan, H., and Feng, K., Effects of Tempering Process on Microstructure and Mechanical Properties of G18NiMoCr3-6, *IOP Conference Series: Materials Science and Engineering*, 493(1), 2019, doi: 10.1088/1757-899X/493/1/012141.
24. Türedi, G.B., Özdemir, U., Murathan, Ö.F., and Kilicli, V., Effect of Tempering Temperatures on Microstructure and Mechanical Properties of AISI 9254 Steel, *International Conference on Material Science and Technology in Cappadocia (IMSTEC'16),* April 6-8, 2016, Nevsehir, Turkey.
25. Huang, B., Lv, H., and Song, Y., Numerical Simulation and Experimental Study of a Simplified Force-Displacement Relationship in Superelastic SMA Helical Springs, *Sensors*, 19(1), 2018, p. 50, doi: 10.3390/s19010050.
26. Liang, C. and Rogers, C., One-Dimensional Thermomechanical Constitutive Relations for Shape Memory Materials, *Journal of Intelligent Material Systems and Structures*, 1990.
27. Budynas, R.G. and Nisbett, J.K., *Shigley's Mechanical Engineering Design,* McGraw-Hill Education, 2008.
28. Shen, H., Zhang, R., Weng, D., Gao, C., Luo, H., and Pan, C., Simple Design Method of Structure with Metallic Yielding Dampers Based on Elastic–Plastic Response Reduction Curve, *Engineering Structures,* 150, 2017, pp. 98–114, doi: 10.1016/j.engstruct.2017.07.047.